EVALUATION OF MODELING ACCURACY OF POWER FREQUENCY FIELD INTERACTIONS WITH THE HUMAN BODY

T. W. Dawson, M. Potter and M. A. Stuchly
University of Victoria, Dept. of Electrical and Computer Engineering
Box # 3055, Stn. CSC, Victoria, BC, Canada, V8W 3P6

Abstract: Heterogeneous voxel models of the human body are used in numerical computations of induced electric fields in tissues. Various numerical methods are used for electric and magnetic field sources under quasi-static conditions. Validation of the computational methods and detailed estimation of errors associated with the modeling are given. Analytic solutions for spheres (homogeneous and layered) and other simple models are used to evaluate modeling accuracy. Sources of inherent errors associated with voxel models (staircase approximation of smooth surfaces) are identified, and methods are presented that decrease the errors.

1. Introduction

Human exposure to electric and magnetic fields at low frequencies including power line frequencies (50 or 60 Hz) results in induction of an electric field and associated current density in tissue. Because of the quasi-static nature of the electromagnetic field at these frequencies, exposure to each field can be considered separately. The total induced values can be found by superposition [1] if required. The relationship between environmental exposures and electrical quantities induced in the body is often termed dosimetry. The default assumption for the dosimetry modeling conducted thus far is that the induced membrane potential is the key transductive event. Induced quantities are also useful for any biological effect that depends on the tissue-induced electric field (or current density). Effects experimentally observed on the bone may serve as an example [2-3]. Dosimetry has also been used as a benchmark in derivation of limits for environmental fields in various exposure guidelines (e.g., [4]).

This work was supported by the NSERC/BCHydro/Bell Mobility/ TransAlta Industrial Research Chair and the EPRI contract WO2966-14.

Additionally, induced quantities at specific sites within the body (e.g., pineal gland, retina, etc.) better characterize the local environment responsible for biological interactions than the external field. This feature helps to assess the plausibility of biological effect or to estimate the quantities associated with any documented effect.

Extensive computations of induced electric field and current density in heterogeneous models of the human body have been performed during the last decade (e.g., [5-12]). Various research groups used different methods, but very similar body models, as reviewed in [13]. For exposures to magnetic fields, two methods have been used, namely the impedance method (IM) [14-15], and the scalar potential finite difference (SPFD) technique [16-17]. The main difference between the two methods (IM and SPFD) is in their computational efficiency. The IM is a vector method, and SPFD is scalar. The impedance method leads to a matrix with 13 non-zero diagonals, while the SPFD gives a matrix with 7 non-zero diagonals. Dimbylow [9] has used both methods and compared their efficiency. The comparison has indicated that 14% less memory is required by the SPFD for the same size of voxels and computation times for SPFD are between 1.5 to 11 times less than for the IM. The greatest time saving is for problems requiring the longest computing times.

For exposures to uniform electric fields, several numerical methods have been used, namely: finite difference (FD), finite difference time domain (FDTD), quasi-static FDTD, and hybrid of quasi-static FDTD with SPFD method. The FDTD simulations have been run at 10 MHz and the results scaled to 60 Hz [15], [11]. This method does not take advantage of the quasi-static nature of the fields. More computationally efficient is quasi-static FDTD [18], or even more so, when this method is hybridized with SPFD [19]. Also, the FD method with nested sub-grids has been successfully used [10]. All computations with the latter methods are performed at 50 or 60 Hz.

The objective of the research presented here is verification of numerical techniques used for high resolution computations for an anatomically representative heterogeneous voxel model of the human body, and evaluation of the inherent errors associated with the voxel model. This verification is performed by comparison of different computed dosimetric measures with those obtained by analytical methods. Simple bodies of revolution are used as tissue models. Evaluations are made for methods used in our laboratory, namely the SPFD, the quasi-static FDTD and the hybrid method. However, since the most significant source of errors is due to the voxel representation of the model, the analyses presented are relevant to other methods.

2. Methodology

2.1 Magnetic Field

The following models are considered in the evaluation: (1) simple homogeneous bodies, namely spheres (circular loop currents) and ellipsoids, (2) double-layered spheres, (3) a sphere with equatorially varying conductivity, and, (4) infinite square-base and other infinite right cylinders. The spheres and ellipsoids are used as a partial verification of numerical codes, basically to evaluate the staircasing error for a given resolution. The symmetry of ellipsoids and spheres in uniform magnetic fields causes the induced fields to depend only on the magnetic vector potential. However, for heterogeneous bodies and arbitrary shapes, the solution consists of two parts, one associated with the scalar potential and the other with the magnetic vector potential. A complete solution is tested with equatorially stratified sphere, for which an analytic solution has become available [20-21]. The infinite cylinders are used to clarify the source of errors associated with voxel models.

In a sphere or, more generally, any circular current loop, a uniform magnetic field induces a current density that can be directly derived from Faraday's law. For a time-harmonic field of radian frequency ω, the magnitude of the current density is

$$J_\phi = \omega\sigma B\frac{r}{2} \tag{1}$$

where $\omega = 2\pi f$, f is the frequency, the subscript ϕ denotes that the current density J is in the equatorial (circumferential) direction, σ is the material (tissue) conductivity, B is the magnetic flux density normal to the current loop, and r is the loop radius.

For a homogeneous ellipsoid with semi-axes $a\times b\times c$, the current paths are ellipses, provided that a uniform magnetic field source is aligned with one of the principal axes of the ellipsoid. The maximum current density is in the cross-section containing the two larger semi-axes with the magnetic field directed along the direction of the shortest axis. If a is the longest semi-axis, and c the shortest, the maximum current density is [22]:

$$J = 2\pi f\sigma B\frac{a^2 b}{a^2+b^2} \tag{2}$$

The average current density has also been computed using the expression given in [22], with a Maple® program to evaluate the elliptic integral required.

In a sphere with an equatorially stratified conductivity profile the conductivity profile is given as [20], [21]:

$$\sigma(\varphi) = \sigma_0 e^{-\lambda\cos(p\varphi)} \tag{3}$$

where $p\in\{1,2\}$ is a periodicity factor, σ_0 is a conductivity amplitude factor, and $\lambda>0$ is a dimensionless conductivity contrast parameter. This distribution has p conductivity maxima and minima as a function of equatorial angle φ, and a maximum conductivity contrast of $e^{2\lambda}$. When $\lambda=0$, the uniform sphere and its associated circular current flow are restored. When $\lambda>0$, the induced current is forced though a conductivity gradient, and a three-dimensional current flow results.

The induced current densities for a uniform field along the x-axis in a conductive square-base cylinder, whose side dimension is much less than the wavelength, can be expressed from the analytic solution given in [23] as:

$$J_y = -j\frac{a\omega\sigma B_x}{\pi^2}\sum_{n=0}^{\infty}\frac{4}{(2n+1)^2}\left(\pm\cos\frac{(2n+1)\pi}{a}y\right)\left(\frac{\sinh\frac{(2n+1)\pi}{a}z}{\cosh\frac{(2n+1)\pi}{2}}\right) \tag{4}$$

and

$$J_z = -j\frac{a\omega\sigma B_x}{\pi^2}\sum_{n=0}^{\infty}\frac{4}{(2n+1)^2}\left(\pm\cos\frac{(2n+1)\pi}{a}z\right)\left(\frac{\sinh\frac{(2n+1)\pi}{a}y}{\cosh\frac{(2n+1)\pi}{2}}\right) \quad (5)$$

where a is the side of the square, σ is the conductivity, and the coordinate system is placed in the center of the cylinder with the x-axis coinciding with the cylinder axis. The sign before the cosine function alternates for consecutive terms.

The principal method used in our high-resolution computations is the SPFD method. It is basically a standard finite-difference method under the quasi-static approximation [6], [8]. In the numerical implementation of the SPFD method, the three-dimensional computational domain is discretized into a uniform set of elementary parallelepipeds or voxels. Within each voxel the electrical properties are assumed constant. The scalar potential method is naturally confined only to the conductor, with potentials defined at the vertices of the voxels. The electric fields are defined as a set of discrete vectors on the staggered array defined by the voxel edges, with field values defined at the edge centers. These are computed *a posteriori,* using finite differences of the potential field. To allow for physical interpretation of the results, electric-field vectors are defined at the voxel centers by averaging the three sets of four parallel-edge components. The magnetic vector potential contribution must also be included. The current density is then computed by multiplying by the voxel conductivity. For comparison purposes, the quasi-static FDTD method is also used [5]. The SPFD method has been selected as the principal method for high-resolution computations for magnetic induction, as it places lower demands on computer resources than the FDTD method. In the SPFD method only the conductor (human body) volume needs to be discretized (this occupies only about 28 % of the volume of the minimal boundary box for an upright posture). In the FDTD method, the human body has to be placed within an air box. The box walls can be as close as one cell away from the body surface. However, the total box size also is increased by a few (about 10) perfectly matched layers (PMLs) to simulate infinite free space. Finally, the FDTD method is vector-based, in contrast to the scalar potential scheme. Therefore, significantly more storage space is required for the FDTD method, even though computer processing time may be comparable for the two methods.

2.2 Electric field

The models considered here are homogeneous or layered spheres. The analytic solutions for homogeneous and layered spheres can be found by solving Laplace's equation in spherical coordinates. The boundary condition

$$\nabla\cdot\left[(\sigma+j\omega\varepsilon)\mathbf{E}\right] = 0 \quad (6)$$

follows from charge conservation at the interface between the two media (free space and outer sphere) and the boundary conditions for the electric fields at the inner sphere interface. Here $\sigma = 0$ for free space, and $\omega\varepsilon << \sigma$ for spheres with conductivity values under the quasistatic approximation. Tangential electric fields must also be continuous across each material interface.

For a layered sphere, the following results are obtained for an applied uniform electric field $\mathbf{E} = \mathrm{E}_o e^{j\omega t}\hat{\mathbf{z}}$:

$$\mathbf{E} = -\mathrm{A}_1\cos\theta\,\hat{\mathbf{r}} + \mathrm{A}_1\sin\theta\,\hat{\theta} \quad \text{for } r < r_1 \quad (7)$$

$$\mathbf{E} = \left(-\mathrm{A}_2 + 2\mathrm{B}_2\frac{r_1^3}{r^3}\right)\cos\theta\,\hat{\mathbf{r}} + \left(\mathrm{A}_2 + \mathrm{B}_2\frac{r_1^3}{r^3}\right)\sin\theta\,\hat{\boldsymbol{\theta}} \quad \text{for } r_1 \le r < r_2 \quad (8)$$

$$\mathbf{E} = \left(-\mathrm{A}_3 + 2\mathrm{B}_3\frac{r_2^3}{r^3}\right)\cos\theta\,\hat{\mathbf{r}} + \left(\mathrm{A}_3 + \mathrm{B}_3\frac{r_2^3}{r^3}\right)\sin\theta\,\hat{\boldsymbol{\theta}} \quad \text{for } r \ge r_2 \quad (9)$$

with

$$\mathrm{A}_1 = 9\alpha\mathrm{E}_0/\sigma_s$$
$$\mathrm{A}_2 = 3\alpha\mathrm{E}_0/\sigma_2$$
$$\mathrm{B}_2 = -3\alpha\mathrm{E}_0\sigma_d/(\sigma_2\sigma_s)$$
$$\mathrm{B}_3 = -\mathrm{A}_3 = \mathrm{E}_o$$

$$\alpha = j\omega\varepsilon_o \Big/ \left[1 + 2\frac{r_1^3\sigma_d}{r_2^3\sigma_s}\right]$$

and $\sigma_d = \sigma_1 - \sigma_2$

$\sigma_s = \sigma_1 + 2\sigma_2$.

Furthermore, r_1 is the radius of the inner sphere, r_2 is the radius of the outer sphere, ε_o is the dielectric constant of free space, and σ_1, σ_2 respectively denote the inner sphere and outer layer conductivity.

For a homogeneous sphere, a simple expression for the interior electric field is obtained

$$\mathbf{E} = \mathrm{E}_{\mathrm{o}} \frac{3j\omega\varepsilon_{\mathrm{o}}}{\sigma}\hat{\mathbf{z}} \tag{10}$$

Current densities are obtained as:

$$\mathbf{J} = \sigma\mathbf{E}. \tag{11}$$

Two methods are used in the numerical computations of induced fields, namely the quasi-static FDTD [18] and the hybrid method [24].

2.3 Numerical Measures

Numerical global measures used in the evaluation of induced electric fields and currents (and also used as dosimetric measures) are the volumetric average, root mean square (rms) and standard deviation values, computed as:

$$\text{Avg E} = \frac{1}{\mathrm{V}}\sum_{\mathrm{i}}^{\mathrm{n}} |\mathrm{E_i}|\Delta\mathrm{v} \tag{12}$$

$$\text{Rms E} = \left[\frac{1}{\mathrm{V}}\sum_{\mathrm{i}}^{\mathrm{n}} |\mathrm{E_i}|^2 \Delta\mathrm{v}\right]^{1/2} \tag{13}$$

$$\text{Std E} = \left[\frac{1}{\mathrm{V}}\sum_{\mathrm{i}}^{\mathrm{n}} \left(|\mathrm{E_i}|^2 - \text{Avg E}\right)^2 \Delta\mathrm{v}\right]^{1/2} \tag{14}$$

where V is the volume of the material (tissue) of a given conductivity, Δv is the voxel volume, and n is the number of voxels in the material. In addition to the global measures, the spatial maximum (max) electric field and current density values for a given voxel are often reported, as are measures designated L99, L95, or L50, denoting the value that is not exceeded in 99 %, 95 % or 50 % of the voxels.

3. Results of Accuracy Evaluation

3.1 Magnetic Field

Comparisons of various measures of induced electric field in homogeneous and layered spheres obtained with numerical (SPFD method) and analytic solutions are shown in Tables 1 and 2. In all cases, a uniform magnetic field of 1 μT at 60 Hz is the source. The uniform sphere has a diameter of 1.22 m and conductivity of 0.25 S/m. Both layered spheres have an outer diameter of 1.22 m and inner diameter of 1.10 m. The inner sphere conductivity is 0.25 S/m, while the outer sphere conductivity is varied to obtain different values of the conductivity contrast.

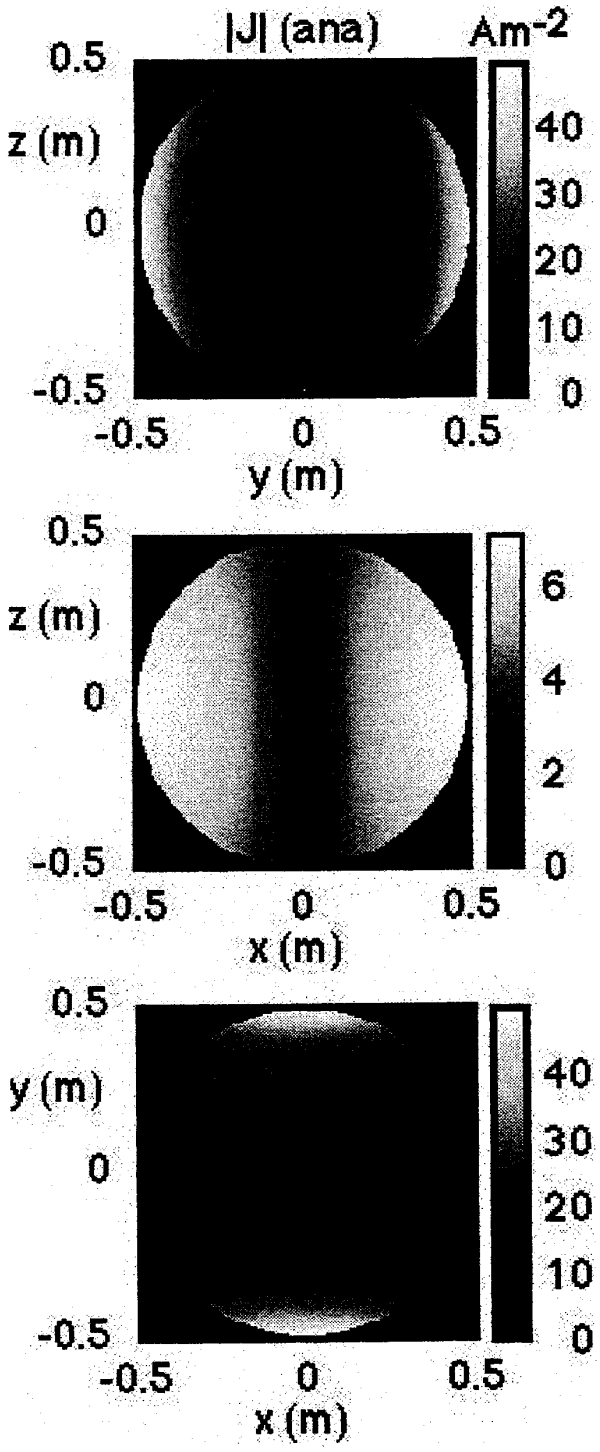

Figure 1a. Magnitude of the current density in a stratified sphere: p=2, λ=1.61, σ=0.2 S/m.

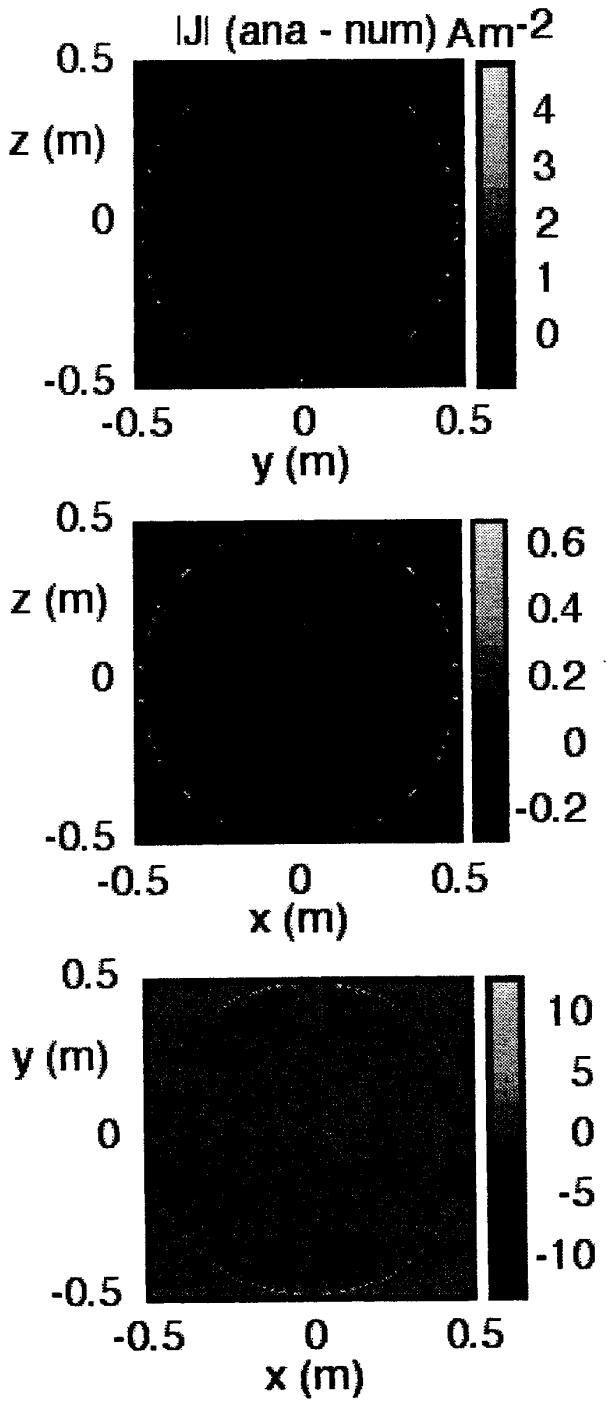

Figure 1b. Absolute difference between analytic and numerical values of the induced current density in the stratified sphere shown in Fig. 1a.

Two versions of the analytic solution are used. All analytical values, except those in Table 1 designated "Analytic integral", are obtained by computing the fields in the centers of the voxels from the analytic solution, and then applying the same statistics (eqs. 12-14) as for the numerical solutions. Excellent agreement between all the measures except the maximum values is apparent for homogeneous and layered spheres. The error in the maximum values increases with improved resolution (Table 1). These errors depend also on the conductivity contrast at the interface, as illustrated by the data for the inner sphere (in Table 2). The increase in L99 for the outer layers is a direct result of large errors in the maximum and a relatively small number of voxels in the layers. Figure 1 shows the current density distributions and the absolute difference between the analytical and numerical solution. The maximum errors in all cases are associated with a few voxels on the interfaces with free space (infinite contrast in conductivity).

For an ellipsoid with $a = 0.1008$ m, $b = 0.2016$ m and $c = 0.8496$ m, and $\sigma = 0.2$ S/m, the error in the average electric field has been computed as equal to 0.2 %, and in the maximum about 23%. The voxel size is 3.6 mm. Very similar errors have been noted for equatorially stratified spheres

To evaluate whether the large error in the maximum values is associated with the SPFD code, the same calculations have been performed with the impedance method code and with our quasi-static FDTD code. Similar large errors have been observed in both codes. Moreover, the positions of the voxels associated with the aberrant values remain the same.

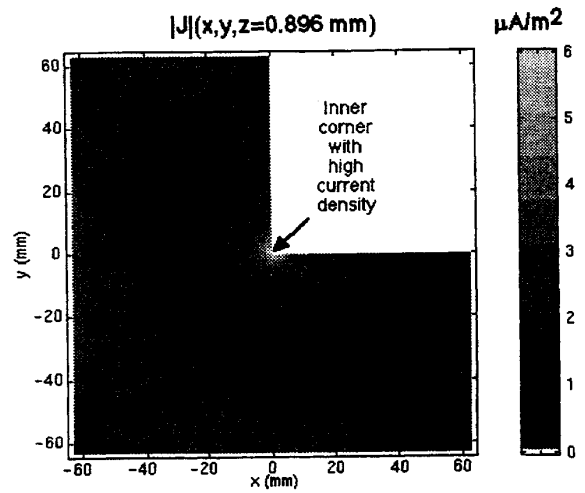

Figure 2. Induced current density in a cylinder with an inner corner.

Table 1. Comparison of the induced electric field (μV/m) in a homogeneous sphere in a uniform magnetic field 1 μT, (60 Hz) for different voxel sizes.

Measure	Analytic integral	7.2 mm voxel Analytic voxel	7.2 mm voxel SPFD	7.2 mm voxel Errors (%)	3.6 mm voxel Analytic voxel	3.6 mm voxel SPFD	3.6 mm voxel Errors (%)	1.8 mm voxel Analytic voxel	1.8 mm voxel SPFD	1.8 mm voxel Errors (%)
Avg	67.73	68.71	68.38	0.50	67.66	67.49	0.25	67.12	67.04	0.12
Rms	72.72	73.78	73.39	0.53	72.65	72.45	0.28	72.07	71.97	0.14
Std	-	26.89	26.65	-	26.46	26.34	-	26.24	26.18	-
L50	69.69	70.05	69.40	0.79	69.51	69.50	0.01	69.11	69.44	0.48
L95	106.9	107.7	106.2	1.41	106.6	105.7	0.85	105.8	105.2	0.57
L99	112.3	113.3	114.9	1.40	112.2	113.3	0.98	111.4	110.9	0.45
Max	115.0	116.4	138.6	19.1	114.7	141.5	23.4	113.9	144.2	26.6

Table 2. Comparison of the induced electric field in two-layer spheres of varying conductivity contrasts. All cases use a 1-μT, 60-Hz uniform magnetic source field and 3.6-mm voxels.

Contrast & Solution	Layer & Error	Avg	Induced Rms	Field L99	Max
Any Analytic	Inner	60.84	65.32	100.8	103.1
	Outer	85.80	89.27	113.9	114.7
2:1 SPFD	Inner	60.79	65.25	100.2	107.2
	Error	0.08%	0.11%	0.60%	4.0%
	Outer	85.30	88.81	120.3	140.7
	Error	0.58%	0.52%	5.6%	22.7%
5:1 SPFD	Inner	60.74	65.19	100.9	115.3
	Error	0.16%	0.20%	0.10%	11.8%
	Outer	85.49	89.05	122.8	139.6
	Error	0.36%	0.13%	7.8%	21.7%
10:1 SPFD	Inner	60.71	65.16	100.9	119.4
	Error	0.21%	0.24%	0.10%	15.8%
	Outer	85.62	89.22	125.1	139.1
	Error	0.21%	0.06%	9.8%	21.3%
50:1 SPFD	Inner	60.68	65.13	101.0	123.7
	Error	0.26%	0.29%	0.20%	20.0%
	Outer	85.79	89.47	128.7	150.5
	Error	0.01%	0.22%	13.0%	31.2%

A comparison of the results obtained with the SPFD code with the analytic solution for a square cylinder has indicated nearly perfect agreement. For a cylinder 1 m x 1 m, the error in the average electric field is 0.01 % and in the maximum less than 1.43 %.

The reason for the behavior of the induced electric field and current density in some voxels due to an inner-corner singularity is shown in Fig. 2. In this case, computations are made for an infinitely long notched square cylinder with the base cross-section as shown in Fig. 2. The magnetic field is parallel to the cylinder axis. At the outer corners of the cylinder in this structure, the electric field tends to zero. However, at the inner corner there is an electric-field singularity. The "congestion" of the induced current close to that corner is intuitively reasonable. The current flow pattern shown in Fig. 2 indicates why the highest current densities in the staircased sphere are in the locations nearest the inside corners close to the "flat" parts of the staircases. In these locations, the highest current density is diverted around the inner corners, just as in the case of the cylinder.

An analytic solution and further explanation of the staircasing errors are given in the Appendix.

3.2 Electric Field

Tables 3 and 4 show comparisons of the induced electric fields in homogeneous and layered spheres for exposure to a uniform 60 Hz electric field of 1 kV/m. Data are computed from analytic solutions (eqs. 7, 8 and 10), and using the quasi-static FDTD and the hybrid method. The homogeneous sphere diameter is 1 m and conductivity is 0.1 S/m. For the layered sphere, the outer layer diameter is 1 m and conductivity 0.1 S/m, the inner diameter is 0.9 m and conductivity is 0.2 or 0.5 S/m for contrast 2:1 and 5:1, respectively. Numerical computations shown in Tables 3 and 4 have been performed with the quasi-static FDTD for 7.2 mm resolution and with the hybrid method for 3.6 mm resolution.

Examination of the comparisons in Tables 3 and 4 indicate that errors on the order of 2-3% are associated with global measures (average, rms). An increase in these errors for the outer sphere is a direct result of large errors in maximum values. Very large errors are associated with maximum values, and similarly to the case for the magnetic field, they do not decrease with increased resolution. Interfaces of lower contrast (Table 4) are associated with lower, but still significant errors in the maximum values of the computed electric field in conductive objects.

The large errors in the maximum values are the result of at least two factors. The first factor is the existence of singularities in charge density at voxel vertices (outside

corners) bordering on free space. The second factor is leakage of the large external electric fields into internal voxels across the air-conductor (high conductivity contrast) boundary.

are inherent in the voxel model of the human body that approximates smooth surfaces with rectangular grids. Such large errors accompany all finite difference based numerical methods,

Table 3. Comparison of the induced electric field (mV/m) in a homogeneous sphere in a uniform electric field for two voxel sizes.

Induced field	7.2 mm voxel			3.6 mm voxel		
	Analytic	Numeric	Errors (%)	Analytic	Numeric	Errors (%)
Avg	0.1001	0.1025	2.4	0.1001	0.1025	2.4
Rms	0.1001	0.1027	2.6	0.1001	0.1027	2.6
Std	0.0000	0.0072	-	0.0000	0.0064	-
L99	0.1001	0.1279	27.8	0.1001	0.1184	11.8
Max	0.1001	0.2878	188	0.1001	0.3593	259

Table 4. Comparison of the induced electric field (μV/m) in two-layer spheres with two values of the conductivity contrast. Uniform electric field is 1 kV/m 60 Hz and voxel dimension is 3.6 mm.

Induced field	Contrast 2:1						Contrast 5:1					
	Inner sphere			Outer sphere			Inner sphere			Outer sphere		
	Ana	Num	Error (%)	Ana	Num	Error (%)	Ana	Num	Error (%)	Ana	Num	Error (%)
Avg	55.0	56.0	1.8	75.3	77.8	3.3	23.4	24.0	2.6	61.1	63.8	4.4
Rms	55.0	56.0	1.8	76.6	80.1	4.6	23.4	24.0	2.6	66.4	69.7	5.0
Std	0.00	1.40	-	14.5	19.0	-	0.00	0.90	-	24.8	28.2	-
L99	55.0	60.3	9.6	105.7	134.1	26.9	23.4	26.4	12.8	110.1	132.6	20.4
Max	55.0	77.2	40.4	110.0	354.6	222	23.4	44.2	88.8	116.9	354.9	204

This leakage into internal regions of the low field magnitude arises from the staircased approximation of smooth surfaces and is due to non-collocated field components (they are defined at voxel edges rather than vertices) combined with the requirement of continuity of tangential electric fields across material boundaries. These two factors combine to produce the much larger errors associated with modeling electric field induction than with modeling magnetic field induction. The charge interpolation from the coarse grid (7.2 mm) to the finer grid (3.6 mm) does not directly contribute to increase in the error in the maximum value. The larger error in the maximum for higher resolution reflects the proximity to the singularity. Additional comments on the source of are given in the Appendix.

4. Modification to Improve the Accuracy

The large errors in maximum values of induced electric field, particularly at the air-tissue interface

Table 5. Errors in the induced electric field in a homogeneous sphere exposed to a uniform magnetic field. The numerical method: quasi-static FDTD with various sub-cell divisions, resolution 3.6 mm.

Induced field	Maximum		Average		Rms	
Cell division	2	8	2	8	2	8
Error (%)	18.7	5.5	0.07	0.1	0.08	0.10

and are much larger for exposures to electric fields than magnetic fields. Modifications to the numerical methods or data post-processing are capable of significantly reducing these errors [25].

For magnetic field exposure sub-cell averaging of material conductivity can be implemented in preprocessing. Such a technique is available in our quasi-static FDTD code [25-26]. Table 5 illustrates the improvements in the accuracy with subdivision into 2 or 8

segments of each voxel. The same homogeneous sphere is modeled as in Table 1. There is no improvement in the already very small errors associated with average measures. The same method can be used in the SPFD code. However, as long as a voxel model of the human body is used this technique is not relevant. Only a human body model, in which organs are represented by surfaces, would be suitable for this error correction.

For electric field exposure, the sub-cell averaging does not improve the accuracy due to the different nature of singularities. The singularity in the charge density occurs in the nodes, electric field components are computed on the voxel edges. Thus, sub-cell averaging cannot account for the error resulting from the lack of collation and the errors due to the enforcement of continuity of tangential components of the electric field (see Appendix). On the other hand, since it is well known that tangential electric fields at the interface of free space with very good conductor tend to zero, this property can be utilized in post-processing to assign zero to electric fields at this interface. The procedure reduces the errors in the maximum electric field at the air interface from about 200 % to 25 % for a resolution of 7.2 mm and estimated about 10 % for a resolution of 3.6 mm.

5. Conclusions

Verification of numerical computer codes and human body models has been performed. Errors have been evaluated by comparing induced electric fields computed by numerical methods with values obtained from analytical solutions. Excellent agreement between the global measures such as the average and rms field values has been obtained for various simple conductive models (e.g. spheres, ellipsoids, and cylinders). Errors of 1-2 % are typical for electric as well as magnetic field exposure.

However, large errors occur in maximum values of induced fields. This is a result of singularities introduced by staircasing smooth surfaces. These errors are the greatest at the free space- conductive body interface, and they are smaller for interfaces between conductors having different conductivity value. The smaller the conductivity contrast, the smaller the error. For voxel human body models these errors are inherent in the model. Methods of reducing the errors in maximum induced fields have been also proposed.

Appendix – Staircasing: Getting the Wrong Answer Right.

Singularities in Low-Frequency Magnetic Induction

It is well-known [27-29], that electromagnetic fields may possess singularities near the vertices of metallic (perfectly conducting) wedges and cones embedded in a dielectric medium. For example, near the vertex of a wedge with interior angle $\alpha < \pi$ (exterior angle $\beta = 2\pi - \alpha > \pi$), the field components transverse to the edge may have singular behavior of the form $\rho^{\nu-1}$. Here ρ is the distance from the edge in a local cylindrical coordinate system and the exponent $\nu = \pi / \beta$.

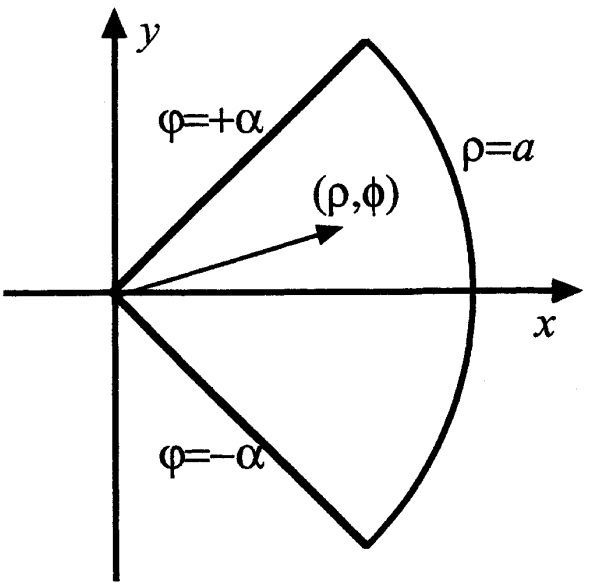

Figure A1. Geometry for a conducting wedge.

Low-Frequency Magnetic Induction

Investigations of edge-singularities typically ignore the possibility of finite metallic conductivity ("the presence of a finite conductivity inevitably increases the analytical complexity of the problem" [29]). Nevertheless, the problem of axial low-frequency magnetic induction in a conducting infinite cylinder with circular sector generator can be solved analytically, and the solution exhibits singular behavior at internal corners. The opening angle of the sector is 2α, as shown in Figure A1. The magnetic source field is $\mathbf{B} = B_0 e^{j\omega t}\hat{\mathbf{z}}$, and a common harmonic time factor will be omitted from here on. The source can be described in polar coordinates by a vector potential, $\mathbf{B} = \nabla \times \mathbf{A}$, where $\mathbf{A} = \frac{1}{2} B_0 \rho \hat{\varphi}$. The electric field is given by $\nabla \times \mathbf{E} = -j\omega \nabla \times \mathbf{A}$, and so has the

representation $\mathbf{E} = -j\omega\mathbf{A} - \nabla\psi$ in terms of a scalar potential ψ. The cylinder is homogeneous with conductivity σ, and consequently the governing current conservation $\nabla \cdot \mathbf{J} = 0$ yields the requirement that ψ be harmonic, $\nabla^2\psi = 0$. Boundary conditions are that the current density, and hence electric field, be tangential to the boundaries. It may be verified post-priori that the solution for the potential can be expressed in the form

$$\psi(\rho,\varphi) = C\sum_{m=1}^{\infty}(-1)^{m-1}R(\kappa_m,\rho)\sin(\kappa_m\varphi) \quad \text{(A1)}$$

where the constant $C = -j\omega B_0 a^2 / 2\alpha$, the eigenvalues are $\kappa_m = (m-1/2)\pi/\alpha$, and the radial functions are

$$R(\kappa,\rho) = \frac{4}{\kappa^2-4}\left[\frac{1}{2}\left(\frac{\rho}{a}\right)^2 - \frac{1}{\kappa}\left(\frac{\rho}{a}\right)^{\kappa}\right] \quad \text{(A2)}$$

Note that this function has a well-defined limit as $\kappa \to 2$. Moreover, since $\kappa_m \geq 0$, the potential is regular. The electric field components E_ρ and E_φ involve the terms $\rho^{-1}R(\kappa,\rho)$ and $\partial R(\kappa,\rho)/\partial\rho$, respectively. These both involve a term ρ^{κ_1-1}, and consequently are singular at $\rho = 0$ if $\kappa_1 < 1$, i.e., if $\alpha > \pi/2$. Thus, the transverse quasi-static electric field is singular at the apex of a conducting reentrant wedge. This is due to the sudden change in direction of the current density along the boundary and associated congestion of current paths near the vertex. The case $\alpha = 3\pi/4$ is of particular relevance to the voxel-based conductivity models. In this case the electric field exhibits a $\rho^{-1/3}$ singularity near a node on a locally two-dimensional inside corner.

It may be noted that in a numerical implementation, the calculated current depends on the conductivity values assigned to the grid edges. The sub-cell modeling algorithm effectively modifies the local edge conductivity values and so influences the computed field values. This mechanism permits the algorithm to partially mitigate unwanted singularity artifacts in the solution

Exact solution of the finite-difference equations.

As an additional check on our solutions of the SPFD equations for magnetic induction, a two-dimensional version was coded using the Maple© symbolic algebra package. A comparison was made for a cylinder with an L-shaped generator of the form shown in Figure 2. The object was discetized into 20x20 squares and a solution obtained using exact rational arithmetic in Maple. A numerical solution was obtained using our three-dimensional SPFD code, using a truncated cylinder containing 20x20x10 voxels. It was found that the resulting solution was almost independent of the vertical coordinate, and the global maximum relative error in electric field modulus between the numerical 3D solution in any horizontal plane and the two-dimensional Maple solution was 0.037%.

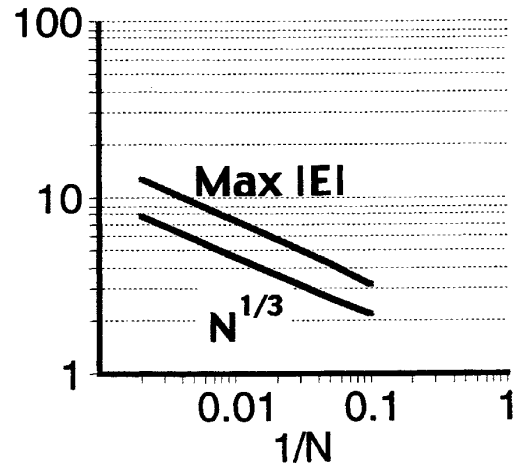

Figure A2. Convergence of the SPFD results near a singularity.

Convergence of the finite-difference solution near a singularity.

Rather than being an artifact, singularities are often a correct and desired part of the solution. Examples include high-frequency full-wave scattering from metallic objects. In such cases, efforts have been made to accommodate the singular nature in numerical methods [30,31].

It has also been noted [29, 30] that unmodified finite difference schemes can converge to the correct singular nature in a brute-force sense. This is also observed in our SPFD code. With the model again consisting of a truncated cylinder with L-shaped generator, as shown in Figure 2, the problem was solved on a NxNx10 grid, for various values of N. The results are shown in Figure A2. The maximum electric field modulus shown correctly tracks the expected $\rho^{-1/3}$ singular nature predicted by the analytic solution.

Singularities in Low-Frequency Electric Induction

As mentioned earlier, for the voxel models under consideration, the case $\alpha = \pi/2$ is relevant. This corresponds to a surface node located on a locally two-

dimensional external edge. Here the transverse external electric field may have singularities of the form $\rho^{-1/3}$. The associated charge density will be infinite at the node, although the total charge in the neighborhood of the node remains finite [29]. Additional singular behavior will be associated with nodes at an outside three-dimensional corner.

Finally, these singularities are purely geometric in nature and are the same as would be observed for the static case. For these reasons, the subcell-modeling algorithm is not capable of mitigating the singular nature.

References

[1] Olsen, R. G., "Power transmission electromagnetics", *IEEE Trans. Antennas Prop,* vol. 35(6), pp. 7-16, 1994.

[2] Rubin, J., K.J. McLeod, M.D. Lnanes, B.D. Catherwood and C. T. Rubin, "Formation of osteoblast-like cells is suppressed by low frequency, low intensity electric fields", *J. Ortho Res.*, vol. 14, pp 7-15, 1996.

[3] Lee, J. H., and K. J. McLeod, "Morphologic responses of osteoblast-like cells in monolayer culture to ELF electromagnetic fields", *Bioelectromagnetics,* vol. 21, pp. 129-136, 2000.

[4] International Commission on Non-Ionizing Radiation Protection (ICNIRP), "Guidelines for limiting exposure to time-varying electric, magnetic and electromagnetic fields (up to 300 GHz)", *Health Physics,* vol. 74, pp. 494-522, 1999.

[5] Dawson, T. W., J. DeMoerloose and M. A. Stuchly, "Comparison of magnetically induced ELF fields in humans computed by FDTD and scalar potential FD codes", *Applied Computational Electromagnetics Society (ACES),* vol. 11, pp. 63-71, 1996.

[6] Dawson, T. W., K. Caputa and M. A. Stuchly, "Influence of human model resolution on computed currents induced in organs by 60 Hz magnetic fields," *Bioelectromagnetics,* vol. 18, pp. 478-490, 1997.

[7] Dawson, T. W., K. Caputa, and M. A. Stuchly, "Effects of skeletal muscle anisotropy on human organ dosimetry under 60 Hz uniform magnetic field exposure", *Phys. Med. Biol.*, vol. 43, pp. 1059-1074, 1998b.

[8] Dawson, T. W. and M. A. Stuchly, "High resolution organ dosimetry for human exposure to low frequency magnetic fields," *IEEE Trans. Magn.*, vol. 34, pp. 1-11, 1998.

[9] Dimbylow, P. J., "Induced current densities from low-frequency magnetic fields in a 2 mm resolution, anatomically realistic model of the body.," *Phys. Med. Biol.*, vol. 43, pp. 221-230, 1998.

[10] Dimbylow, P. J., "Current densities in a 2mm resolution anatomically realistic model of the body induced by low frequency electric fields", *Phys. Med. Biol.,* vol. 45, pp. 1013-1022, 2000.

[11] Furse, C. M. and O. P. Gandhi, "Calculation of electric fields and currents induced in a mm-resolution human model at 60 Hz using the FDTD model," *Bioelectromagnetics*, vol. 19, pp. 293-299, 1998.

[12] Gandhi, O. P., "Some numerical methods for dosimetry: Extremely low frequencies to microwave frequencies," *Radio Science*, vol. 30, pp. 161-177, 1995.

[13] Stuchly, M. A. and T. W. Dawson, "Interaction of low frequency electric and magnetic fields with the human body", *Proc. IEEE,* vol. 88, pp.643-664, 2000.

[14] Gandhi, O. P., and J. F. De Ford, "Calculation of EM power deposition for operator exposure to RF introduction heaters", *IEEE Trans. Electromagnetic Compat.,* vol. 30, pp. 63-68, 1988.

[15] Gandhi, O. P. and J.-Y. Chen, "Numerical dosimetry at power line frequencies using anatomically based models," *Bioelectromagnetics Supplement*, vol. 1, pp. 43-60, 1992.

[16] Dawson, T. W. and M. A. Stuchly, "Analytic validation of a three-dimensional scalar-potential finite-difference code for low-frequency magnetic induction.," *Applied Computational Electromagnetic Society (ACES)*, vol. 11, pp. 72-81, 1996.

[17] Dawson, T. W., K. Caputa and M. A. Stuchly, "High-resolution organ dosimetry to human exposure to low-frequency electric fields", *IEEE Trans Power Delivery,* vol. 13, pp. 366-376, 1998a.

[18] DeMoerloose, J., T. W. Dawson and M. A. Stuchly, "Application of finite difference time domain algorithm to quasi-static field analysis," *Radio Science,* vol. 32, pp. 329-342, 1997.

[20] Dawson, T. W. and M. A. Stuchly, "An analytic solution for verification of computer models for low-

frequency magnetic induction," *Radio Science,* vol. 32, pp. 343-367, 1997.

[21] Dawson, T. W., "Analytic solution for low-frequency magnetic induction in an equatorially stratified sphere: Horizontal excitation," *Radio Science,* vol. 32(5), pp. 1761-1776, 1997.

[22] Kaune, W. T., J. L. Guttman and R. Kavet, "Comparison of coupling of humans to electric and magnetic fields with frequencies between 100 Hz and 100 kHz," *Bioelectromagnetics,* vol. 18, pp. 67-76, 1997.

[23] McLeod, B. R., A. A. Pilla and M. W. Sampsel, "Electromagnetic fields induced by Helmholtz aiding coils inside saline-filled boundaries," *Bioelectromagnetics,* vol. 4, pp. 357-370, 1983.

[24] Dawson, T. W., J. DeMoerloose and M. A. Stuchly, "Hybrid finite-difference method for high-resolution modeling of low-frequency electric induction in humans", *J. Computational Physics,* vol. 136, pp. 640-653, 1997b.

[25] Potter, M. E., M. Okoniewski and M.A. Stuchly, "Low frequency finite difference time domain (FDTD) for modeling of induced fields in humans close to line sources", *J. Comput. Physics,* vol. 162, pp. 82-103, 2000.

[26] Okoniewski, M. and M. A. Stuchly, " A study of the handset antennas and human body interaction", *IEEE Trans. Microwave Theory Tech.,* vol. 44, pp. 1884-1897, 1996.

[27] Meixner., J, "The Behaviour of Electromagnetic Fields at Edges", *IEEE. Trans. Antennas Propagation*, vol.20, pp.442-446, 1972.

[28] Mittra R. and S. W. Lee, "Analytic Techniques in the Theory of Guided Waves", Macmillan Series in Electrical Science, Roger F. Harrington (Ed.), Macmillan, New York, 1971

[29] Van Bladel J, "Singular Electromagnetic Fields and Sources", IEEE/OUP Series on Electromagnetic Wave Theory, Donald G. Dudley (Ed.), Oxford University Press (Oxford) and IEEE Press (New Jersey), 1991.

[30] Mur G, "The Modeling of Singularities in the Finite-Difference Approximation of the Time-Domain Electromagnetic-Field Equations", *IEEE. Trans. Microwave Theory Techniques*, vol.29, pp.1073-1077, 1981.

[31] Lubuma,J.M.-S. and S. Nicaise, "Finite Element Method for Elliptic Problems with Edge-Singularities", *J. Comp. Appl. Math.*, vol.106, pp.145-168, 1999.